A Direct Classical Trajectory Study of HCl Elimination from the 193 nm Photodissociation of Vinyl Chloride

Emilio Martínez Núñez* and Antonio Fernández-Ramos

Departamento de Química Física, Facultad de Química, Universidad de Santiago de Compostela, 15782 Santiago de Compostela, Spain

Saulo A. Vázquez,† F. Javier Aoiz, and Luis Bañares

Departamento de Química Física, Facultad de Química, Universidad Complutense, 28040 Madrid, Spain

Received: March 31, 2003; In Final Form: June 12, 2003

Direct AM1 with specific reaction parameters (AM1-SRP) trajectory calculations were performed to investigate the photodissociation of vinyl chloride at 193 nm. Marked differences were found between the trajectories run from the transition states to the products for the four-center (4C) and three-center (3C) dissociation channels. The average internal energy of HCl is found to be about 2.5 times larger for the 4C channel. The calculated translational and HCl vibrational distributions, especially those obtained with a quasi-classical normal-mode sampling method, are in good agreement with the experimental data. The results are consistent with a concerted but nonsynchronous 3C mechanism, producing a lifetime for vinylidene to acetylene isomerization in line with the experimental observations. The theoretical HCl rotational distributions are in reasonable agreement with experiment, although they do not support the experimental interpretation of Lin et al. [*J. Chem. Phys.* **2001**, *114*, 160], who attributed low-*J* and high-*J* components to the 4C and 3C channels, respectively.

I. Introduction

The photodissociation dynamics of chloroethylenes has been long studied in the literature during the last thirty years.[1−28] The ultraviolet absorption in these molecules is characterized by a strong band near 190 nm dominated by a $\pi^* \leftarrow \pi$ transition. At wavelengths < 200 nm, there is sufficient energy for several dissociation pathways to compete. The elimination of HCl, H_2, H, and Cl(^2P_J) have all been identified as primary dissociation processes in the 193 nm photodissociation of the simplest chloroethylene molecule, vinyl chloride (VCl).

Berry[3] determined the population of vibronic states of HCl up to $v = 4$ for various chloroethylenes in a chemical laser study. He concluded that HCl is produced primarily via a four-center (4C) elimination channel and rationalized the observed nonstatistical vibrational distribution of HCl according to an impulse mechanism in which the localized energy is partitioned between internal energy of HCl and relative translational energy of the fragments. Infrared emission spectroscopy by Moss et al.[8] showed substantial excitation in the acetylene/chloroacetylene partner fragments and a high degree of rotational excitation in the HCl products. Donaldson and Leone,[11] using a Fourier transform infrared (FTIR) spectrometer, found a somewhat cooler HCl vibrational distribution than that reported by Berry.[3] Gordon and co-workers[12] performed pump−probe experiments in a molecular beam containing VCl and detected Cl and HCl after photolysis at 193 nm using (2+1)-resonance-enhanced multiphoton ionization (REMPI) followed by time-of-flight (TOF) mass spectrometry detection. They found a bimodal rotational distribution for HCl ($v = 0$) with temperatures corresponding to 340 and 22 600 K, but Boltzmann-like distributions corresponding to rotational temperatures of 2100 and 1850 K for the $v = 1$ and $v = 2$ states of HCl, respectively. Very recently, Lin et al.[28] reported fully resolved vibration−rotation emission spectra of HCl in the spectral region 2000−3310 cm^{-1}. Contrary to the observations of Reilly et al.,[12] they obtained bimodal rotational distributions for all of the vibrational levels studied ($v = 1-6$). Upon the basis of statistical phase space theory (PST), separate statistical ensamble (SSE), and impulse model approaches, they concluded that the observed high-*J* and low-*J* components correspond to HCl(v,J) produced from three-center (3C) and 4C elimination channels, respectively.

Gordon's group[21] also reported state-resolved translational energy distributions of Cl and HCl. They found that the product translational energy distribution is nonstatistical, in agreement with the results of a previous photofragment translational spectroscopy (PTS) study.[10] To explain the experimental data, they proposed that the 3C elimination and the isomerization from vinylidene (CCH_2) to acetylene (HCCH) occur in a concerted but nonsynchronous fashion. The isomerization is expected to be rapid enough to share its exothermicity with nearby HCl fragments so that HCl departs with augmented vibrational and translational energies. Blank et al.,[26] using photofragment translational spectroscopy, found that all channels, except the Cl dissociation, are consistent with competition on the ground electronic state following internal conversion from the optically prepared state. The translational energy distribution for HCl peaked at about 12 kcal mol^{-1} and had an average value of 18 ± 1 kcal mol^{-1}, in agreement with previous studies.

On the theoretical side, Morokuma and co-workers performed extensive calculations of the ground-state potential energy surface (PES) for all reaction channels of VCl and dichloro-

* To whom correspondence should be addressed. E-mail address: uscqfemn@cesga.es. Fax: +34 981 595012.

† Permanent address: Departamento de Química Física, Universidad de Santiago de Compostela, 15782 Santiago de Compostela, Spain.

10.1021/jp034824p CCC: $25.00
Published on Web 09/03/2003

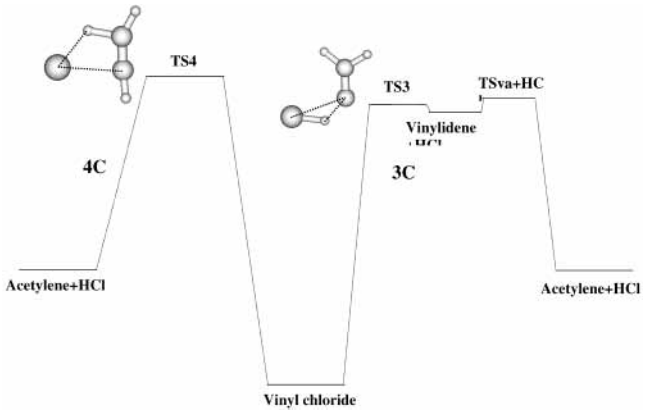

Figure 1. Schematic potential energy diagram showing the main (3C and 4C) HCl elimination channels involved in the photodissociation of vinyl chloride.

ethylene.[18,19] They examined all 3C, 4C, and migration mechanisms for molecular elimination. For VCl, the calculated barriers for the 3C and 4C elimination of HCl are 69.1 and 77.4 kcal mol^{-1}, respectively. Except for the 3C channel, that study predicts that the dissociation pathways have substantial exit barriers and that the 3C channel is the dominant channel for HCl production, in agreement with experimental work.[13,21] Also, the barrier to H-atom migration was determined to be slightly below the 3C elimination barrier, suggesting that partial H-atom scrambling may precede dissociation. This is consistent with the indistinguishable rotational state distributions found for HCl produced from the deuterated and normal VCl.[15]

In this work, we present dynamical calculations for the HCl elimination channel from the 193 nm photodissociation of VCl. The aim is to corroborate or clarify or both the conclusions derived from the reported experimental studies. To the best of our knowledge, this is the first dynamical study on this prototypical system. Specifically, product energy distributions for HCl elimination occurring through the 3C and 4C channels were calculated by direct classical trajectories on two different semiempirical potential energy surfaces (PESs), one for each channel (see Figure 1 for the description of the 4C and 3C channels). The parameters of the AM1 Hamiltonian were modified to achieve good accordance between the ab initio PES of Riehl and Morokuma[18] and the semiempirical AM1 calculations. This is known as AM1 with specific reaction parameters (AM1-SRP).[29] The trajectories for each channel were started from the relevant transition states (TS3 and TS4, see Figure 1), considering that a microcanonical ensemble is maintained at least up to the transition-state region. This seems to be a good approximation because the reaction barriers for VCl dissociation are high enough to ensure rapid vibrational energy redistribution at the reactant phase space (in comparison with the rate of reaction), at least at the 193 nm excitation considered here. In addition, results extracted from classical trajectories initiated at the barrier should be reliable because comparisons between classical and quantum dynamics have shown[30] that classical dynamics gives accurate results for a direct process like motion down a potential energy barrier provided that the trajectories are initialized with the correct quasi-classical conditions.

II. Potential Energy Surfaces

In this section, we present the model PESs employed for each channel. Semiempirical restricted Hartree-Fock (RHF)−AM1 PESs were parametrized (AM1-SRP) for each reaction channel to fit ab initio and experimental data of those features relevant to the dynamics.[29]

For the four-center channel, we used the ab initio data of Riehl and Morokuma[18] to fit a semiempirical AM1-SRP PES of the form

$$V = (1 - f)V_1 + fV_2 \tag{1}$$

where V_1 and V_2 are different AM1-SRPs that describe properly different regions of the PES and f is the switching function

$$f = 0.5\{1 + \tanh[a(r_{CCl} - h)]\} \tag{2}$$

which varies from 0 (near the transition-state region) to 1 (at the asymptotic product limit). Thus, near the transition state (low values of r_{CCl}), the potential is almost V_1, while as the reaction proceeds and r_{CCl} becomes larger, V_2 dominates. In eq 2, parameter a controls the rate at which f is "turned on", and h is the point at which f is "turned on" halfway. The values were $a = 2$ Å^{-1} and $h = 4.5$ Å.

V_1 was chosen after minimization of the following expression:

$$W_{E_r}(E_1 - E_1^0)^2 + W_F(\omega_F - \omega_F^0)^2 + \sum_i W_r(r_i - r_i^0)^2 \tag{3}$$

where each term involves the AM1-SRP minus ab initio values (QCISD(T)/6-311+G(d,p) for energies and MP2/6-31G(d,p) for geometries and frequencies).[18] E_1 is the reverse barrier height for reaction (the energy difference between TS4 and the products), ω_F is the imaginary frequency at TS4, and r_i are the CC, CCl, CH_i, and H_iCl bond distances at this transition state (H_i being the H atom attached to Cl). The weights in eq 3 are $W_E = 1$ kcal^{-2} mol^2, $W_F = 3 \times 10^{-5}$ cm^2, and $W_r = 2$ Å^{-2}.

V_2 was fitted to reproduce the experimental or ab initio geometries or both and frequencies of the HCl and acetylene products, and the function minimized to obtain the SRPs was

$$\sum_i W_{F_i}(\omega_{F_i} - \omega_{F_i}^0)^2 + \sum_i W_r(r_i - r_i^0)^2 \tag{4}$$

where ω_{F_i} and r_i are the HCl and acetylene vibrational frequencies and bond distances, respectively. The weights in eq 4 are $W_F = 1 \times 10^{-3}$ cm^2 and $W_r = 1$ Å^{-2}.

For the 3C channel, we only considered one AM1-SRP PES because this is a more involved PES in which either acetylene or vinylidene can be formed, making it difficult a treatment compared with that used for the 4C channel. The function minimized in this case to obtain the SRPs was

$$W_E[(E_1 - E_1^0)^2 + (E_2 - E_2^0)^2 + (E_3 - E_3^0)^2] + W_F(\omega_F - \omega_F^0)^2 + \sum_i W_r(r_i - r_i^0)^2 \tag{5}$$

where E_1, E_2, and E_3 are the relative energies between TS3 and HCl + acetylene, TS3 and HCl + vinylidene, and TSva and HCl + vinylidene, respectively (see Figure 1), ω_F is the imaginary frequency at TS3, and r_i are the CCl, CH_i, and H_iCl bond distances at this transition state (H_i being the H atom attached to Cl). The weights in eq 5 are $W_E = 1$ kcal^{-2} mol^2, $W_F = 1 \times 10^{-5}$ cm^2, and $W_r = 100$ Å^{-2}.

Each of the preceding fits included 30 parameters that were optimized by using a gradient-based least-squares minimization procedure considering upper and lower bounds of ±15% of the original AM1 values. The optimized parameters for each channel are collected in Table 1. Table 2 shows a comparison between experimental or ab initio results or both for some attributes of the vinyl chloride ground-state PES and those obtained with the present model PESs. Overall, the differences between the

TABLE 1: Parameters Employed in the AM1-SRP Hamiltonians for the 4C and 3C Reaction Channels of HCl Elimination

	4C		
parameter	V_1	V_2	3C
U_{ss}(H)	−11.567 373 5	−11.498 995 0	−12.271 672 4
β_s(H)	−6.766 470 59	−6.877 598 74	−4.325 355 18
Z_s(H)	1.198 770 75	1.280 748 12	1.118 219 03
α(H)	2.830 442 16	2.804 501 25	2.920 370 57
G_{ss}(H)	13.580 335 4	12.385 471 7	9.039 852 34
U_{ss}(C)	−50.155 628 4	−54.369 949 1	−52.340 830 2
U_{pp}(C)	−41.278 036 5	−39.970 766 8	−39.614 237 6
β_s(C)	−16.611 582 6	−14.678 541 6	−16.281 550 8
β_p(C)	−7.765 598 8	−7.232 968 35	−8.650 228 36
Z_s(C)	1.678 441 18	1.678 441 18	1.901 992 09
Z_p(C)	1.781 167 65	1.937 883 42	1.552 665 89
α(C)	2.560 880 92	2.560 880 92	2.565 647 72
G_{ss}(C)	11.386 129 7	11.753 029 6	11.943 817 2
G_{sp}(C)	11.504 410 3	11.435 590 3	11.229 129 9
G_{pp}(C)	10.947 039 9	12.741 999 6	11.884 407 5
G_{p2}(C)	9.869 520 15	9.840 000 00	9.916 751 86
H_{sp}(C)	2.517 480 06	2.437 290 07	1.701 000 02
U_{ss}(Cl)	−111.279 103	−123.668 249	−109.805 796
U_{pp}(Cl)	−76.410 185 9	−70.432 258 6	−76.640 103 9
β_s(Cl)	−27.029 541 2	−20.905 469 5	−21.436 713 3
β_p(Cl)	−14.637 215 6	−15.735 006 6	−14.786 514 8
Z_s(Cl)	3.631 376 03	4.165 188 22	3.502 825 22
Z_p(Cl)	2.388 318 7	1.889 887 04	2.352 182 37
Z_d(Cl)	1.150 000 0	1.150 000 00	1.300 000 00
α(Cl)	2.910 609 93	3.024 465 26	3.124 307 57
G_{ss}(Cl)	16.021 979 6	17.284 499 3	11.891 735 5
G_{sp}(Cl)	13.160 000 0	12.054 560 0	13.160 000 0
G_{pp}(Cl)	11.435 600 2	12.994 999 9	11.435 599 8
G_{p2}(Cl)	9.970 000 27	10.299 010 2	9.975 981 97
H_{sp}(Cl)	2.420 000 08	2.724 920 04	2.430 164 0

ab initio (or experimental) data and the AM1-SRP PESs are rather small. The maximum deviations (absolute error of ∼2 kcal mol^{-1}) between the ab initio and the semiempirical barriers are those involved in the acetylene−vinylidene isomerization process. Regarding the geometries at the transition states, the comparison is very good, major differences appearing for the CCl distance at TS3. The products acetylene and HCl are very well reproduced by the 4C PES and reasonably well by the three-center PES (in the four-center PES the product geometries and frequencies were employed in the parametrization procedure). Taking into account the complexity of the global PES, the comparison between the ab initio (or experimental) and AM1-SRP results is satisfactory, and therefore, our model PESs seem to be appropriate for dynamical purposes.

Figure 2 shows contour maps of the 3C and 4C PESs drawn by varying the CCl and H_iCl bond distances and constraining the other coordinates to their values at the corresponding saddle point. As can be seen, the 4C channel exhibits a large number of contour lines in the direction of product formation because of its large exit barrier, whereas the contour map of the 3C channel depicts a typical case of a reaction with a rather "loose" transition state. On the other hand, the H_i−Cl distance at the 4C transition state TS4 (1.79 Å, see Table 2) is significantly longer than the corresponding value at TS3 (1.45 Å). Obviously, these substantial differences between the 3C and 4C exit barriers will have important implications on the dynamics of product formation.

III. Trajectory Computational Details

The trajectories were initiated at transition states TS3 and TS4 by using two sampling methods. The first is a quasiclassical rigid-rotor/normal-mode method (hereafter S1), described in detail elsewhere,[32,33] which allows one to obtain a microcanonical ensemble of rovibrational states at the barrier by assigning n_i, J, and K quanta to a given degree of freedom, using the following probability function:

$$P(n_i,J,K) = \frac{N^{ts}_{n_i,J,K}}{N^{ts}_{tot}} \tag{6}$$

where N^{ts}_{tot} is the total number of rovibrational states at the barrier and $N^{ts}_{n_i,J,K}$ is the barrier sum of states with a given degree of freedom having a fixed number of quanta. In the present study, the total angular momentum was restricted to zero.

The second barrier sampling method employed here (S2) is based on the efficient microcanonical sampling of Nyman, Nordholm, and Schranz,[34,35] which takes into account the full anharmonicity and vibrational coupling of the PES. A Markov chain is propagated by moving at random some (or all) of the Cartesian coordinates of the system, confining the sampling to the configuration space spanned by the normal mode coordinates at the barrier.[36] For each accepted configuration, random atomic momenta are generated to match the total energy of the system. With the generated momenta, the vibrational energy in each normal mode is calculated and compared to the corresponding zero-point vibrational energy (ZPVE). If the energy of every normal mode is greater than the corresponding ZPVE, the phase space point is accepted. This sampling method is similar to those employed by Nyman et al.[37] and Marks[38] and is explained in more detail in ref 36.

Each ensemble of trajectories was excited at the energy corresponding to a photon excitation of 193 nm, the photon wavelength employed in the experimental work of Berry,[3] Donaldson and Leone,[11] Reilly et al.,[12] Blank et al.,[26] and Lin et al.[28] Each run consisted of 5000 trajectories, which were integrated by using a combined fourth-order Runge−Kutta and sixth-order Adams−Moulton predictor−corrector algorithm with a fixed step size of 0.05 fs, using an extensively adapted version of the GENDYN program,[39] which incorporates the relevant subroutines of MOPAC7.0.[40,41] During the integration of trajectories, energy conservation of better than four digits was obtained. When the HCl−acetylene (vinylidene) center-of-mass distance reached 10 Å, the trajectories were halted and the distributions of product internal and recoil translational energies were computed. The distributions of translational energy were fitted by using the method of Legendre moments, and the HCl vibrational quantum numbers were calculated by the Einstein−Brillouin−Keller (EBK) quantization of the action integral.

IV. Results and Discussion

A. Translational Energy Distributions. Figure 3 shows the translational energy distributions (TEDs) obtained here for the 3C and 4C channels using the two different excitation models (S1 and S2). For the 4C channel, the distributions peak at energies between 30 and 40 kcal mol^{-1}, which is consistent with the very large reverse barrier (52 kcal mol^{-1}) of this reaction channel. In cases such as this, the fragments rapidly dissociate with considerable translational energy, having little chance to randomize the available energy at the barrier, which results in nonstatistical product energy partitioning. For channel 3C, the most probable translational energy is in the range 10−15 kcal mol^{-1}. This result is, at first sight, unexpected because this channel has a very small reverse barrier (only 1.5 kcal mol^{-1}), which should lead to a near-statistical TED with a maximum probability near zero, as predicted, for example, by a prior distribution[42] (see Figure 3a). However, if the 3C process

TABLE 2: Some Attributes of the AM1-SRP PES[a] in Comparison with ab Initio Results and Experiment

	4C		3C	
parameter	ab initio[b]/expt[c]	AM1-SRP	ab initio[b]/expt[c]	AM1-SRP
		Exit-Channel Energetics		
E_1	52.3	52.4	44.3	44.7
E_2			1.5	−0.8
E_3			3.7	5.7
		Transition States		
r_{CCl}	2.43	2.43	2.58	2.49
r_{CH_i}	1.26	1.26	1.36	1.35
r_{CC}	1.25	1.25	1.30	1.30
r_{H_iCl}	1.79	1.79	1.44	1.45
ω_{TS}	1844*i*, 267, 385, 609, 707, 747, 749, 887, 1577, 1904, 3432, 3505	1847*i*, 353, 468, 584, 915, 956, 1080, 1111, 1746, 2012, 3423, 3518	575*i*, 183, 387, 491, 714, 817, 894, 1290, 1437, 1743, 3225, 3335	509*i*, 183, 379, 485, 491, 722, 861, 1218, 1286, 1894, 2674, 2744
		Products		
r_{HCl}	1.27; 1.27*	1.27	1.27; 1.27*	1.23
r_{CC}	1.22; 1.20*	1.22	1.22; 1.20*	1.19
r_{CH}	1.06; 1.06*	1.07	1.06; 1.06*	1.08
ω_{HCl}	2991*	2983	2991*	2414
ω_{HCCH}	612* (2), 730* (2), 1974*, 3289*, 3374*	610 (2), 770 (2), 1972, 3305, 3364	612* (2), 730* (2), 1974*, 3289*, 3374*	430 (2), 941 (2), 2237, 3030, 3099

[a] Energies in kcal mol^{-1}, frequencies in cm^{-1}, and distances in Å. [b] From ref 18, MP2/6-31G(d,p) results for frequencies and geometries and QCISD(T)/6-311+G(d,p) calculations at the MP2/6-31G(d,p) optimized geometries for energies. [c] Experimental values (identified with an asterisk) from ref 31.

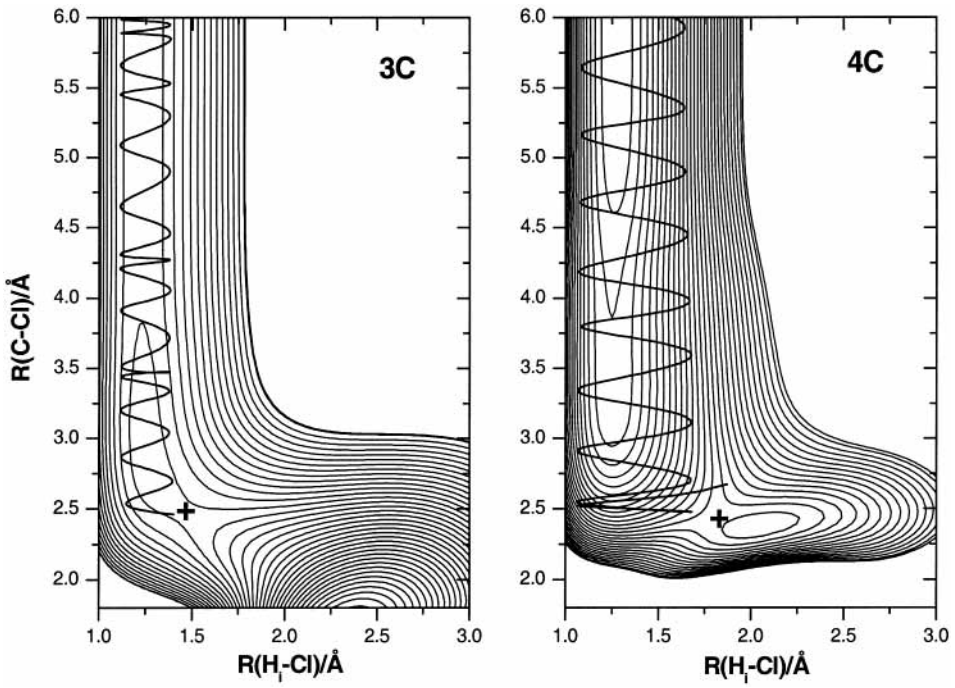

Figure 2. Countour maps of the PESs for the 3C and 4C channels. The plots are drawn by varying R_{CCl} and R_{H_iCl} with the other coordinates fixed to the values at the corresponding saddle point. Contour space is 3 kcal mol^{-1}. The symbol + denotes the position of the saddle point. To illustrate the larger HCl vibrational excitation involved in the 4C mechanism, a typical trajectory, projected onto the subspace spanned by the R_{CCl} and R_{H_iCl} coordinates, is represented in each panel by a bold line.

occurs concertedly, as first proposed by Gordon and coworkers,[21] the isomerization of singlet vinilydene to acetylene may share its exothermicity with the nearby HCl fragment, leading to enhanced translational (and vibrational) energy. The present results support Gordon's assumption. Furthermore, the lifetime of vinylidene was calculated to lie between 58 fs (from the S2 calculations) and 77 fs (from S1),[43] values which are in the range of 40−200 fs estimated from line width analysis of negative ion photodetachment experiments.[44] To corroborate that a significant fraction of the translational energy comes from the concerted (but nonsynchronous) isomerization process, we have performed an additional trajectory calculation for the 3C channel on a modified PES, in which the energy of TSva (the transition state for the vinylidene−acetylene isomerization) was artificially shifted up to 60 kcal mol^{-1} above vinylidene to ensure that all of the trajectories finish as vinylidene. The TED thus obtained is shown in Figure 3a (labeled as 3C*). As seen in the figure, the 3C* TED, which is substantially different from that obtained using the "true" PES, peaks close to zero and agrees quite well with the prior statistical distribution.

Figure 3 also shows a comparison between the present results and the experimental determinations.[26] To calculate a weighted

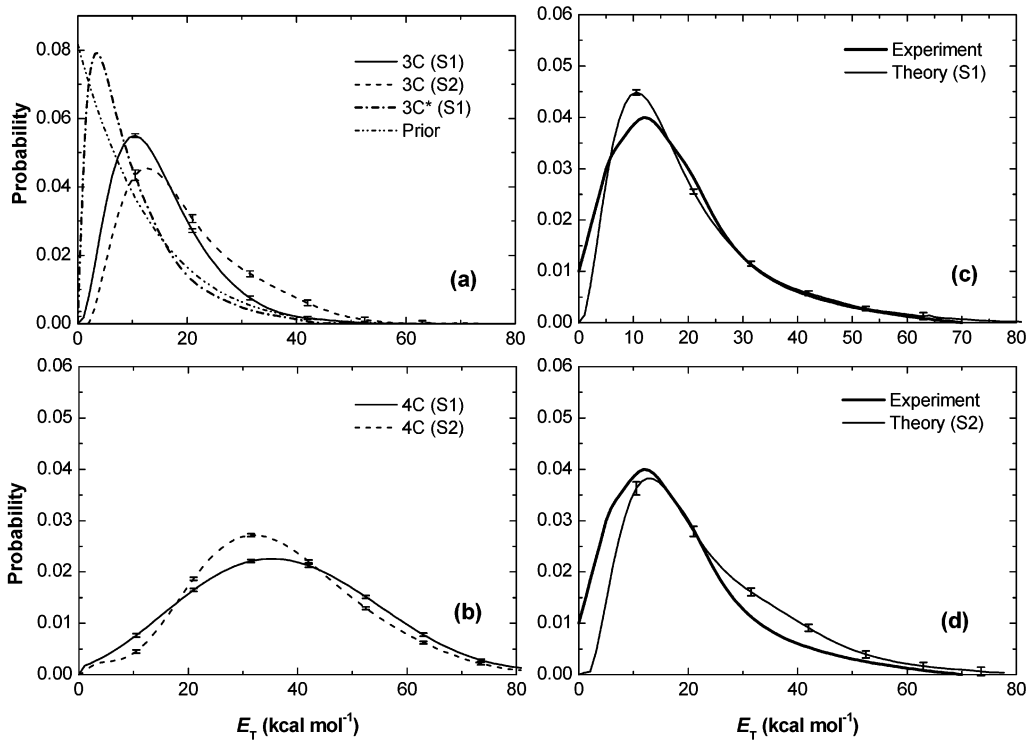

Figure 3. Calculated translational energy distributions for the photodissociation of VCl at 193 nm using the S1 and S2 excitation models for (a) the 3C channel and (b) the 4C channel. For the 3C channel, the prior distribution and the trajectory results obtained with an unrealistic PES (with a high E_2 value; see text) are also shown for comparison. The total translational energy distributions calculated as weighted contributions from the 4C and 3C channels (see text) are displayed for (c) excitation model S1 and for (d) excitation model S2, along with the experimental curve of Blank et al.[26] (solid thick line). In both cases, the experimental distribution was normalized to have the same area as the theoretical ones.

TABLE 3: Vibrational Populations of HCl[a] Obtained for the 4C and 3C Reaction Channels from the Vinyl Chloride Photodissociation at 193 nm

	4C		3C		total theory[b]		expt		
							ref	ref	ref
v	S1	S2	S1	S2	S1	S2	3	11	28
0	0.71	0.76	1.43	1.87	1.37 ± 0.05	1.72 ± 0.07	1.17		
1	1.00	1.00	1.00	1.00	1.00 ± 0.05	1.00 ± 0.07	1.00	1.00	1.00
2	1.29	0.96	0.71	0.61	0.76 ± 0.05	0.65 ± 0.05	0.90	0.62	0.87
3	1.33	0.86	0.43	0.35	0.53 ± 0.05	0.42 ± 0.05	0.80	0.50	0.74
4	1.14	0.75	0.24	0.22	0.34 ± 0.05	0.28 ± 0.05	0.63	0.37	0.61
5	0.90	0.57	0.14	0.04	0.24 ± 0.03	0.12 ± 0.02			0.42
6	0.62	0.46	0.07	0.04	0.13 ± 0.03	0.09 ± 0.02			0.26

[a] Normalized to $v = 1$. [b] Total vibrational populations calculated as weighted contributions from the four-center and three-center channels (see text for details). Errors are evaluated at the 99% confidence limit.

TABLE 4: Product Energy Partitioning Obtained for the 4C and 3C Reaction Channels from the Photodissociation of Vinyl Chloride at 193 nm[a]

	4C		3C		total theory[b]		
energy	S1	S2	S1	S2	S1	S2	expt
E_{trans}	37.0	37.8	15.3	19.5	19.6	23.2	18 ± 1[c]
$E_{rot,HCCH}$	6.7	9.2	9.2	10.3	8.7	10.1	
$E_{vib,HCCH}$	32.4	30.2	77.9	75.8	68.8	66.7	
$E_{rot,HCl}$	17.0	16.2	10.4	9.8	11.7	11.1	9.3[d]
$E_{vib,HCl}$	29.1	28.8	9.4	6.8	13.4	11.1	13.8[e]; 18.0[d]

[a] Energies (in kcal mol^{-1}) are with respect to the ZPVE of the products. [b] Total vibrational populations calculated as weighted contributions from the 4C and 3C channels (see text for details). [c] Taken from ref 26. [d] Taken from ref 28. [e] Taken from ref 3.

(total) contribution from the results for the 3C and 4C channels, we used a 3C/4C branching ratio of 4/1, which is between the experimental estimations (2.3/1 and 3/1 in refs 7 and 15, respectively) and the RRKM calculation (6.7/1) of Lin et al.[28] As can be seen, the results for sampling S1 are in very good agreement with the experimental TED. Both curves peak at ~12 kcal mol^{-1}, and the average energies are about 18−19 kcal mol^{-1}. The minor contribution from the 4C channel is responsible for the long tail decay of the total TED in comparison with that of the 3C channel.

B. HCl Vibrational Populations. The vibrational state distributions obtained in this work using both excitation models (S1 and S2) for the two elimination channels are listed in Table 3, together with the available experimental data.[3,11,28] The vibrational distribution for the 4C channel is inverted, with the greatest populations in $v = 3$ and $v = 1$ for the S1 and S2 samplings, respectively, while that for the 3C channel is nearly Boltzmann. Thus, the vibrational energy content of HCl is 3−4 times greater for the 4C than for the 3C channel (see Table 4). This is a consequence of the different nature of the 4C and 3C channels. As mentioned before, the 4C channel presents two important features that lead to a high vibrational content in the nascent HCl species. First, this channel has a large reverse barrier (52 kcal mol^{-1}), part of which is converted into vibrational energy of HCl. And second, the HCl distance at TS4 (1.8 Å) is significantly stretched in comparison with the equilibrium bond length (1.3 Å) of the HCl molecule. Quantum-mechanically, this corresponds to a high Franck−Condon projection of the transition-state wave function onto the product HCl wave function for high vibrational levels.[45] Qualitatively, our results can be visualized as depicted in Figure 2, in which a typical trajectory is projected onto the plane defined by the R_{CCl} and R_{HiCl} coordinates. As seen in the figure, the trajectory on the 4C PES exhibits large-amplitude oscillations, as compared to the 3C trajectory, indicating that the HCl fragment departs with significant vibrational excitation.

The comparison between theory and experiment is reasonably good (especially with the results of Donaldson and Leone[11]),

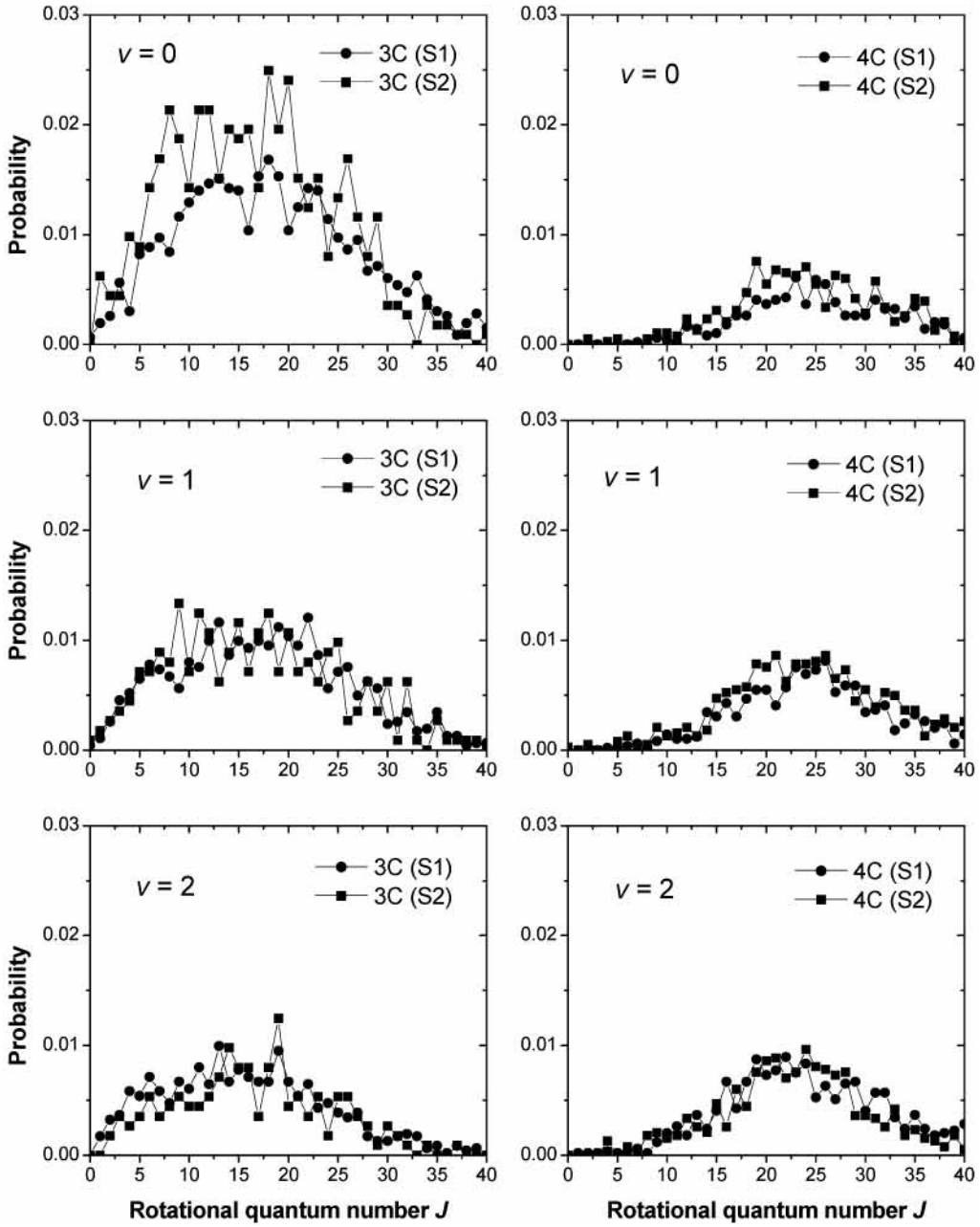

Figure 4. Theoretical rotational state distributions for HCl(v=0−2) using the S1 and S2 excitation models for the 3C channel (left panels) and 4C channel (right panels) from the photodissociation of VCl at 193 nm.

although our vibrational distribution is slightly cooler than those obtained experimentally. This is clearly seen in the average vibrational energy content of HCl (Table 4): 11−13 kcal mol^{-1} calculated here vs 14−17 kcal mol^{-1} estimated experimentally. Of the two initialization methods, the S1 leads to a better agreement with experiment. The differences between the S1 and S2 sampling methods and their influence on the product energy distributions have been discussed in detail elsewhere.[36,46,47]

C. HCl Rotational Populations. Figure 4 depicts the rotational distributions for $v = 0-2$ obtained in this study using both S1 and S2 sampling methods for the 3C and 4C channels. For both channels, the maximum rotational quantum number J is slightly higher than 30. However, while the average HCl rotational energy for the 3C channel is around 10 kcal mol^{-1}, that for the 4C channel is 16−17 kcal mol^{-1}. In addition, for the 3C channel, all rotational levels with J ranging from 0 to 30 are populated, whereas for the 4C channel only rotational levels with $J > 10$ are substantially populated. As can be seen in the figure, both sampling methods yield very similar rotational distributions for all vibrational states of HCl.

The theoretical rotational distributions for $v = 1-6$ are compared in Figure 5 with those obtained experimentally by Lin et al.[28] For simplicity, given the good agreement found between the S1 and S2 results, we only show in this figure the results obtained for the S1 initialization. As for the TEDs, the theoretical rotational distributions shown in Figure 5 were obtained by weighting the 3C and 4C contributions using a 3C/4C branching ratio of 4/1. In addition, to compare the experimental and theoretical results, both sets of results were scaled using a single value in such a way that the total population summed over all rovibrational states experimentally probed is the same. Both the theoretical and the experimental results of Lin et al.[28] give an average HCl rotational energy around 10 kcal mol^{-1} (see Table 4), although the theoretical rotational distributions are less populated for low-J values. It is important to note that in the experimental distributions of Reilly et al.[12]

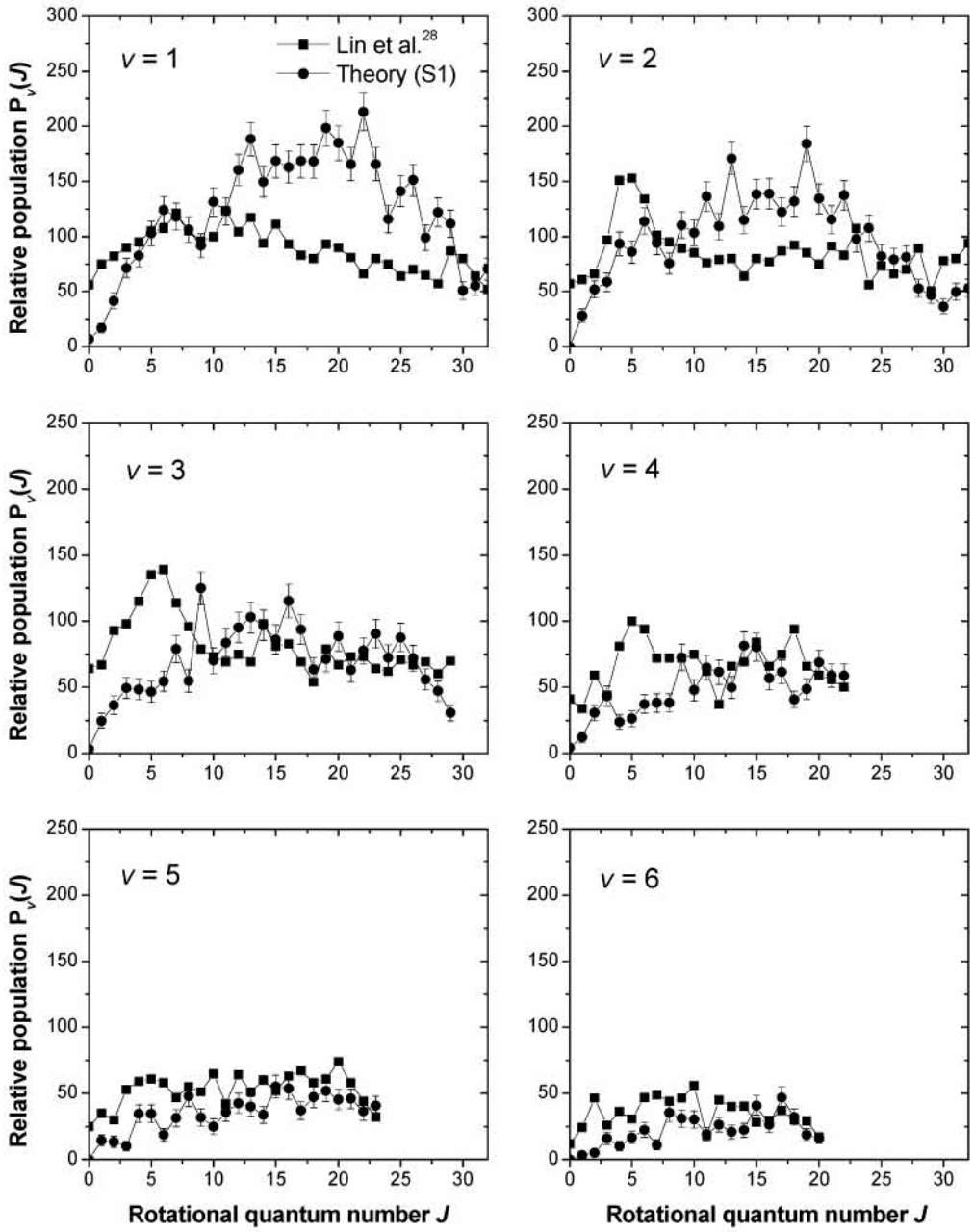

Figure 5. Relative rotational distributions of HCl(v=1−6). The total theoretical distributions were calculated by using the S1 initialization and a 3C/4C branching ratio of 4/1. A single scaling factor for all distributions was used to make the comparison.

(not shown) there is an absence of population for high-*J* states, which may arise from the lack of sensitivity of the REMPI scheme for these transitions of HCl, as stated by Lin et al.[28] These latter authors[28] adjusted their distributions to biexponential functions to yield two rotational temperatures and denoted the two components as high-*J* and low-*J* contributions. On the basis of PST, SSE, and impulse model calculations, they attributed the high-*J* and low-*J* components to the 3C and 4C elimination channels, respectively. By contrast, our calculations do not predict bimodal distributions for $v = 1-6$ (neither for $v = 0$), at least apparently. Their low-*J* component (with values of *J* less than 10) has an average rotational energy of less than 1 kcal mol^{-1}, which is much smaller than the value 16−18 kcal mol^{-1} obtained here for the 4C channel. Additionally, the fraction of 4C trajectories with $J < 10$ is negligible. Therefore, the present results are not consistent with the interpretation of Lin et al.[28] We note that they used an impulse model in which only the TS4 geometry and the eigenvector of the imaginary frequency play a role on the computed product properties. Their model rules out the possibility that the "dissapering modes" (which are correlated with product rotational and translational motion) contribute to the rotational energy of the products. More involved methods, such as the statistical adiabatic impulse model of Mourdant et al.,[45] should be employed for a more reliable prediction of the product energies. If the rotational distributions had bimodal character, as suggested by Lin et al.,[28] it might be due to subtle effects in the PES. For this reason, we are currently performing MP2/6-31G(d,p) direct trajectories on the HCl elimination from VCl photodissociation. The preliminary calculations for the 4C channel give an average HCl rotational energy of 18 kcal mol^{-1} and indicate that the percentage of trajectories with $J < 10$ is small, in agreement with the AM1-SRP computations. A full account on the ab initio direct trajectories will be reported in a separate paper.

V. Summary and Conclusions

Product energy distributions were obtained for the HCl elimination from the VCl photodissociation at 193 nm by direct AM1-SRP trajectory calculations. The trajectories were run from the transition states to the products for the four-center and three-center dissociation channels. The product energy distributions calculated for these channels showed significant differences among them. Particularly, the 4C mechanism is highly non-statistical with a large percentage of the reverse barrier going into product translational energy. For the 3C channel, the trajectory calculations are consistent with a concerted but nonsynchronous mechanism, previously proposed by Gordon and co-workers,[21] and the calculated lifetime for vinylidene to acetylene isomerization agrees with the experimental observations.[44] This concerted mechanism allows some of the energy involved in the reverse isomerization barrier to be released as translational energy of the fragments.

The vibrational and rotational populations of HCl for the 3C and 4C channels are substantially different. The average internal energy of HCl is about 2.5 times larger for the 4C than for the 3C channel.

The calculated translational distributions, especially for S1, are in good accord with experiment. This agreement supports the concerted nature of the 3C mechanism, as well as a branching ratio 3C/4C $\approx$ 4/1. The rotational energy distributions obtained here are in reasonable agreement with experiment, although the trajectory results are at odds with the interpretation of Lin et al.[28] They obtained bimodal distributions and claimed that the low-J distribution arises from the 4C process, whereas in the present calculations only a very low fraction of trajectories initiated at TS4 led to low-J values in the nascent HCl species.

Acknowledgment. E.M.N. and A.F.-R. thank the Spanish Ministry of Science and Technology for their Ramón y Cajal research contracts. S.A.V. thanks Xunta de Galicia for a grant to support his sabbatical stay at Universidad Complutense de Madrid. Financial support from the Spanish Ministry of Science and Technology (Grants BQU2000-0462 and BQU2002-04627-C02-02) and from the European Commission within the RT Network (Contract No. HPRN-CT-1999-00007) is gratefully acknowledged.

References and Notes

(1) Fujimoto, T.; Rennert, A. M.; Wijnen, M. H. J. *Ber. Bunsen-Ges. Phys. Chem.* **1970**, *74*, 282.
(2) Molina, M. J.; Pimentel, G. C. *J. Chem. Phys.* **1972**, *56*, 3988.
(3) Berry, M. J. *J. Chem. Phys.* **1974**, *61*, 3114.
(4) Ausubel, R.; Wijnen M. H. J. *Int. J. Chem. Kinet.* **1975**, *7*, 739.
(5) Ausubel, R.; Wijnen M. H. J. *J. Photochem.* **1975**, *4*, 241.
(6) Ausubel, R.; Wijnen M. H. J. *Z. Phys. Chem.* **1976**, *100*, 175.
(7) Reiser, C.; Lussier, F. M.; Jensen, C. C.; Steinfield, J. I. *J. Am. Chem. Soc.* **1979**, *101*, 350.
(8) Moss, M. G.; Ensminger, M. D.; McDonald, J. D. *J. Chem. Phys.* **1981**, *74*, 6631.
(9) Kato, S.; Morokuma, K. *J. Chem. Phys.* **1981**, *74*, 6285.
(10) Umemoto, M.; Seki, K.; Shinohara, H.; Nagashima, U.; Nishi, N.; Kinoshita, M.; Shimada, R. *J. Chem. Phys.* **1985**, *83*, 1857.
(11) Donaldson, D. J.; Leone, S. R. *Chem. Phys. Lett.* **1986**, *132*, 240.
(12) Reilly, P. T. A.; Xie, Y.; Gordon, R. J. *Chem. Phys. Lett.* **1991**, *178*, 511.
(13) Mo, Y.; Tonokura, K.; Matsumi, Y.; Kawasaki, M.; Sato, T.; Arikawa, T.; Reilly, P. T. A.; Xie, Y.; Yang, Y.; Huang, Y.; Gordon, R. J. *J. Chem. Phys.* **1992**, *97*, 4815.
(14) He, G.; Yang, Y.; Huang, Y.; Gordon, R. J. *J. Phys. Chem.* **1993**, *97*, 2186.
(15) Huang, Y.; Yang, Y.; He, G.; Gordon, R. J. *J. Chem. Phys.* **1993**, *99*, 2752.
(16) Sato, K.; Shihira, Y.; Tsunashima, S.; Umemoto, H.; Takayanagi, T.; Furukawa, K.; Ohno, S. *J. Chem. Phys.* **1993**, *99*, 1703.
(17) Huang, Y.; He, G.; Yang, Y.; Hashimoto, S.; Gordon, R. J. *Chem. Phys. Lett.* **1994**, *229*, 621.
(18) Riel, J.-F.; Morokuma, K. *J. Chem. Phys.* **1994**, *100*, 8976.
(19) Riel, J.-F.; Musaev, D. G.; Morokuma, K. *J. Chem. Phys.* **1994**, *101*, 5942.
(20) Suzuki, T.; Tonokura, K.; Bontuyan, L. S.; Hashimoto, N. *J. Phys. Chem.* **1994**, *98*, 13447.
(21) Huang, Y.; Yang, Y.; He, G.; Hashimoto, S.; Gordon, R. J. *J. Chem. Phys.* **1995**, *103*, 5476.
(22) Sato, K.; Tsunashima, S.; Takayanagi, T.; Yokoyama, K.; Fujisawa, G.; Yokoyama, A. *Chem. Phys. Lett.* **1995**, *232*, 357.
(23) He, G.; Yang, Y.; Huang, Y.; Hashimoto, S.; Gordon, R. J. *J. Chem. Phys.* **1995**, *103*, 5488.
(24) Sato, K.; Tsunashima, S.; Takayanagi, T.; Fujisawa, G.; Yokoyama, A. *J. Chem. Phys.* **1997**, *106*, 10123.
(25) Tonokura, K.; Daniels, L. B.; Suzuki, T.; Yamashita, K. *J. Phys. Chem. A* **1997**, *101*, 7754.
(26) Blank, D. A.; Sun, W.; Suits, A. G.; Lee. Y. T., North, S. W.; Hall, G. E. *J. Chem. Phys*. **1998**, *108*, 5414.
(27) Cho, S. H.; Park, W. H.; Kim, S. K.; Choi, Y. S. *J. Phys. Chem. A* **2000**, *104*, 10482.
(28) Lin, S.-R.; Lin, S.-C.; Lee, Y.-C.; Chou, Y.-C., Chen, I.-C.; Lee, Y.-P. *J. Chem. Phys*. **2001**, *114*, 160.
(29) González-Lafont, A.; Truong, T.; Truhlar, D. G. *J. Phys. Chem.* **1991**, *95*, 4618.
(30) Untch, A.; Schinke, R.; Cotting, R.; Huber, J. R. *J. Chem. Phys.* **1993**, *99*, 9553.
(31) Data from NIST Standard Reference Database 69-July 2001 Release: *NIST Chemistry WebBook*, http://webbook.nist.gov/chemistry.
(32) Doubleday, C.; Bolton, K.; Peslherbe, G. H.; Hase, W. L. *J. Am. Chem. Soc.* **1996**, *118*, 9922.
(33) Bolton, K.; Hase, W. L.; Peslherbe, G. H. *Modern Methods for Multidimensional Dynamics in Chemistry*; World Scientific: Singapore, 1998.
(34) Nyman, G.; Nordholm, S.; Schranz, H. W. *J. Chem. Phys.* **1990**, *93*, 6767.
(35) Schranz, H. W.; Nordholm, S.; Nyman, G. *J. Chem. Phys.* **1991**, *94*, 1487.
(36) Martínez-Núñez, E.; Vázquez, S. A.; Varandas, A. J. C. *Phys. Chem. Chem. Phys.* **2002**, *4*, 279.
(37) Nyman, G.; Rynefors, K.; Holmlid, L. *J. Chem. Phys*. **1988**, *88*, 3571.
(38) Marks, A. J. *J. Chem. Phys.* **1998**, *108*, 1438.
(39) Tompson, D. L. *GENDYN program*; Oklahoma State University.
(40) Stewart, J. P. P. *MOPAC7.0*, a General Molecular Orbital Package; Quantum Chemistry Program Exchange, Indiana University: Bloomington, IN, 1993; p 455.
(41) Stewart, J. P. P. *J. Comput. Chem.* **1989**, *10*, 209.
(42) Baer, T.; Hase, W. L. *Unimolecular Reaction Dynamics*; Oxford University Press: New York, 1996.
(43) The lifetime was calculated as the time needed to reach the top of the TSva barrier, using a test based on the geometrical parameters of this transition state.
(44) Ervin, K. M.; Ho, J.; Lineberg, W. C. *J. Chem. Phys.* **1989**, *91*, 5974.
(45) Mourdaunt, D. H.; Osborn, D. L.; Neumark, D. M. *J. Chem. Phys.* **1998**, *108*, 2448.
(46) González-Vázquez, J.; Martínez-Núñez, E.; Fernández-Ramos, A.; Vázquez, S. A. *J. Phys. Chem. A* **2003**, *107*, 1398.
(47) Martínez-Núñez, E.; Estévez, C. M.; Flores, J. R.; Vázquez S. A. *Chem. Phys. Lett.* **2001**, *348*, 81.